催化学报
2011 Chinese Journal of Catalysis Vol. 32 No. 4

文章编号: 0253-9837(2011)04-0555-11 国际版 DOI: 10.1016/S1872-2067(10)60212-4 研究论文: 555~565

WO_3/ZnO复合光催化剂的制备及其光催化性能

余长林[1,*], 杨 凯[1], 舒 庆[1], YU Jimmy C[2], 操芳芳[1], 李 鑫[1]

[1]江西理工大学材料与化学工程学院, 江西赣州 341000

[2]香港中文大学化学系, 香港

摘要: 采用沉淀-研磨法制备了一系列不同WO_3含量的WO_3/ZnO复合光催化剂, 应用N_2物理吸附、X射线衍射、扫描电镜、傅里叶变换红外光谱、紫外-可见光谱和光致发光谱等手段对催化剂进行了表征, 并以λ = 365 nm的紫外光为光源, 评价了该催化剂光催化降解酸性橙II的活性, 考察了WO_3的复合对WO_3/ZnO样品光催化性能的影响. 结果表明, 当复合2%WO_3, 并于600 °C焙烧时, 所制备的WO_3/ZnO催化剂活性最高, 比纯ZnO的提高了约一倍. 合适的煅烧温度可以提高催化剂结晶度, 而WO_3的复合可抑制ZnO晶粒的长大, 提高催化剂比表面积和改善催化剂表面羟基数量, 并可抑制光生电子与光生空穴的复合, 从而显著提高其光催化脱色活性.

关键词: 氧化钨; 复合; 氧化锌; 光催化; 酸性橙 II

中图分类号: TB321, O643 **文献标识码**: A

收稿日期: 2010-12-08. 接受日期: 2010-12-29.

*通讯联系人. Tel: (0797) 8312431; E-mail:yuchanglinjx@163.com

基金来源: 国家自然科学基金(21067004); 江西省自然科学基金(2010GZH0048); 江西省教育厅青年科学基金(GJJ10150); 固体表面物理化学国家重点实验室开放基金厦门大学(200906).

本文的英文电子版(国际版)由Elsevier出版社在ScienceDirect上出版(http://www.sciencedirect.com/science/journal/18722067).

Preparation of WO_3/ZnO Composite Photocatalyst and Its Photocatalytic Performance

YU Changlin[1,*], YANG Kai[1], SHU Qing[1], YU Jimmy C[2], CAO Fangfang[1], LI Xin[1]

[1]*School of Materials and Chemical Engineering, Jiangxi University of Science and Technology, Ganzhou 341000, Jiangxi, China*

[2]*Department of Chemistry, The Chinese University of Hong Kong, Hong Kong, China*

Abstract: A series of WO_3/ZnO composite photocatalysts with different WO_3 concentrations were prepared by a precipitation-grinding method followed by calcination at different temperatures. The prepared samples were characterized by N_2 physical adsorption, X-ray diffraction, scanning electron microscopy, Fourier transform infrared spectroscopy, UV-visible spectroscopy, and photoluminescence spectroscopy. The photocatalytic activity of the samples was evaluated by photocatalytic degradation of acid orange II under UV light (λ = 365 nm) irradiation. The results showed that at the optimal calcination temperature of 600 °C, the WO_3/ZnO composite photocatalyst with 2 wt% concentration of WO_3 showed about doubled photocatalytic activity compared to pure ZnO. The increase in the photocatalytic activity could be attributed to the coupling of WO_3, which suppressed the growth of ZnO particles, increase of the surface area and increased amount of surface OH groups of the sample. The presence of WO_3 also restrained the recombination rate of e^-/h^+ pairs.

Key words: tungsten oxide; coupling; zinc oxide; photocatalysis; acid orange II

Received 8 December 2010. Accepted 29 December 2010.

**Corresponding author. Tel: +86-797-8312431; E-mail: yuchanglinjx@163.com*

This work was supported by the National Natural Science Foundation of China (21067004), Natural Science Foundation of Jiangxi Province, China (2010GZH0048), Research Foundation of Education Bureau of Jiangxi Province, China (GJJ10150), and Open Project Program of State Key Laboratory of Physical Chemistry of Solid Surfaces (Xiamen University), China (200906).

English edition available online at Elsevier ScienceDirect (http://www.sciencedirect.com/science/journal/18722067).

半导体光催化氧化技术具有操作简单、反应条件温和、能耗低及二次污染少等优点,因而在环境治理领域引起广泛关注[1~4]. ZnO是一种禁带宽度约为3.1 eV的n型半导体,广泛应用于纤维、化妆品、陶瓷、玻璃和建材等领域,同时它具有一定的光催化性能,可将各种易挥发性有机污染物最终氧化为CO_2和H_2O等无机物,也可氧化除去水中几乎所有的有机污染物,因此它的光催化作用近来引起人们的重视[5,6]. 与TiO_2相比, ZnO光催化剂的催化效率不高[7],且易发生光腐蚀而导致稳定性低. 目前,提高ZnO光催化性能的主要方法有: (1)通过制备方法改变其物理结构性质,如改变其粒径或形貌[8~10]; (2)采用表面贵金属沉积[11~12]、金属离子掺杂[13]、半导体复合[14~15]或非金属掺杂[16]等方法改变其能级结构,提高其光催化效率. 其中半导体复合可利用两种半导体的互补性质,即两种半导体材料之间的能级差有效分离电荷,达到促进光生电子和空穴对的分离、转移和传递的作用,从而可以抑制光生电子和空穴的复合,这是提高光催化剂活性和稳定性的有效途径之一. WO_3同样是一种n型半导体,其禁带宽度略小,为2.7 eV左右,且其价带和导带能级位置与ZnO不同.

本文考察了复合不同含量的WO_3对ZnO结构、表面性质、光生电子和空穴对的分离效率及光催化降解酸性橙II反应性能的影响.

1 实验部分

1.1 催化剂的制备

称取3.00 g钨酸钠(AR,上海国药集团)和0.05 g十六烷基溴化铵(CTAB, AR,上海清析化工有限公司)溶于10 ml去离子水中,磁力搅拌使其溶解,然后缓慢滴加入10 ml 1.5 mol/L硝酸溶液,搅拌2 h. 将反应液离心沉降,用水、无水乙醇洗涤2~3次,将钨酸于干燥箱中80 °C干燥2 h,得到黄钨酸备用. 称取3.67 g $Zn(NO_3)_2$ (AR,上海国药集团)与0.10 g CTAB溶于50 ml水中,另将1.31 g碳酸钠溶于50 ml水中制成碳酸钠溶液,再缓慢加入$Zn(NO_3)_2$溶液中,搅拌反应1 h,过滤,用水和无水乙醇洗涤,于80 °C干燥,得到碱式碳酸锌,再与不同含量黄钨酸研磨0.5 h,然后在马弗炉中以3 °C/min升到不同温度煅烧2 h,得到WO_3/ZnO复合催化剂. 样品中的元素含量用PW2424型X射线荧光分析仪(Panalytical)测定.

1.2 催化剂的表征

样品比表面积的测定在美国Quantachrome公司NOVA 4000型自动物理吸附仪上进行. 将样品在350 °C下脱气2 h后,以N_2为吸附质于–196 °C恒温吸附. 比表面积由N_2吸附等温线结合BET方程求得. 样品的X射线衍射(XRD)分析在Bruker D8型X射线衍射仪(Cu K_α, λ = 0.154178 nm)上进行,扫描范围2θ = 10°~80°,管电压30 kV,管电流15 mA. 用XL30型扫描电子显微镜(SEM,荷兰飞利浦)观察样品整体形貌,同时对部分样品进行能量弥散X射线(EDX)元素分析(美国EDax Genesis型能谱仪). 样品的紫外可见吸收光谱(UV-Vis)在日本岛津UV-2550型紫外可见分光光度计上获得,以$BaSO_4$做参照. 样品的傅里叶变换红外(FT-IR)光谱在美国热电公司Nicolet-470型红外光谱仪上测定,分辨率为4 cm^{-1}. 样品先于250 °C燥4 h,再于KBr混合压片制样. 为了表征光催化剂的光生电子空穴对的重组和寿命,使用Spex 500M型荧光光谱仪在室温下测定样品的光致发光谱(PL). 测试时,样品超声分散于无水乙醇中.

1.3 催化剂的评价

光催化反应在自制的光催化反应器中进行. 光反应器中心光源为15 W 365 nm的汞灯(Cole-Parmer仪器公司). 在光催化反应中,染料酸性橙II溶液的初始浓度为20 mg/L,溶液体积为80 ml,催化剂用量为50 mg. 反应前,含催化剂的染料悬浮液在暗处搅拌吸附40 min以达平衡,然后打开光源. 在光照的不同时间段取样1~2 ml,高速离心分离后,除去里面的催化剂颗粒,用721型分光光度计在484 nm处测定上层清液的吸光度. 根据下式计算酸性橙II的降解率D,即$D = (A_0 - A)/A_0$,其中A_0和A分别为染料初始和降解后的吸光度.

2 结果与讨论

2.1 催化剂的表征结果

2.1.1 XRD结果

图1(a)为纯ZnO和不同WO_3含量的WO_3/ZnO样品的XRD谱. 由图可见,所有样品均出现对应于六方晶系纤锌矿结构的ZnO(100), (002), (101), (102), (110), (103), (200), (112)和(201)晶面的特征衍射峰

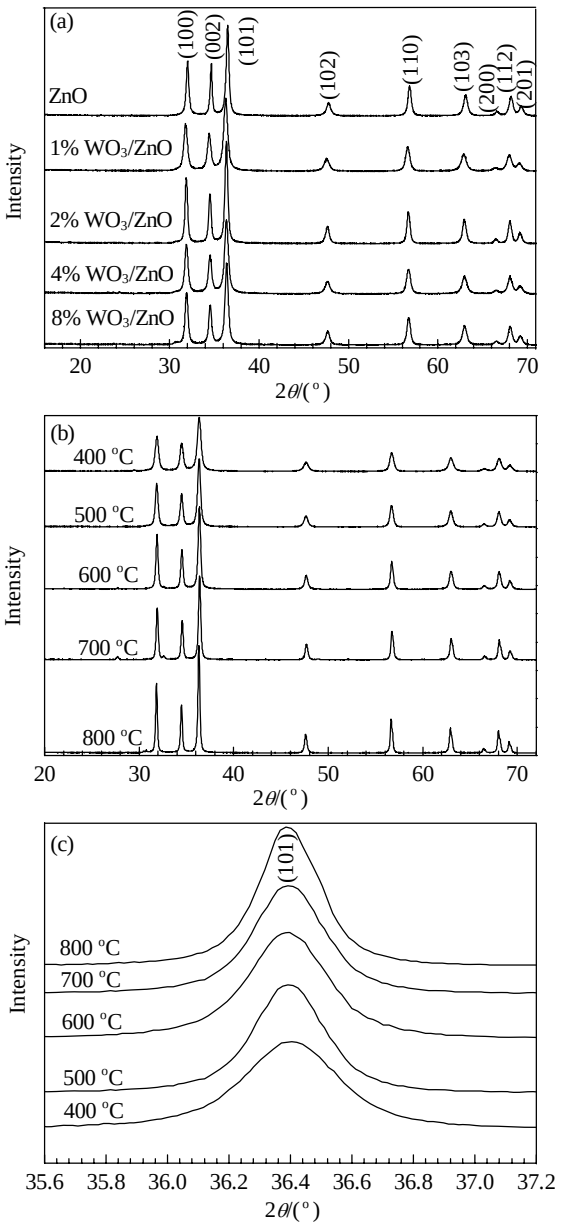

图 1 不同样品的 XRD 谱

Fig. 1. XRD patterns of the samples. (a) ZnO and WO_3/ZnO with different WO_3 contents calcined at 500 °C; (b) 2%WO_3/ZnO calcined at different temperatures; (c) (101) plane of 2%WO_3/ZnO calcined at different temperatures.

(JCPDS 36-1451), 峰形尖锐, 表明样品均具有很高的结晶度. 在所有 WO_3/ZnO 样品上均未出现 WO_3 的特征衍射峰. 这主要是由于 WO_3 处于高度分散状态或其浓度较低[17], 超出了 XRD 的检测极限. 图 1(b) 为不同温度煅烧的 2%WO_3/ZnO 样品的 XRD 谱. 可以看出, 各样品衍射峰位置没有发生改变, 说明在此过程中没有新物相生成, 只是随着煅烧温度的升高, 相应产物的 (101) 晶面衍射峰强度逐渐增加. 表明样品结晶度逐渐增加.

为了考察 WO_3 的复合和锻烧温度对 ZnO 样品晶粒大小的影响, 根据 ZnO 的最强特征衍射峰 (101) 晶面的半峰宽数据, 按 Scherrer 公式计算得 ZnO 的平均晶粒尺寸, 结果见表 1. 由表 1 可见, WO_3 的复合使 ZnO 粒径有所减小, 表明 WO_3 的存在可在一定程度上抑制 ZnO 粒子的长大. 这可能是由于 W^{6+} 离子半径 (0.068 nm) 与 Zn^{2+} 的半径 (0.083 nm) 比较接近, 部分 W^{6+} 离子进入到 ZnO 的晶格中, 从而抑制了 ZnO 晶粒的长大[18]. 将不同温度煅烧的 2%WO_3/ZnO 样品在 (101) 晶面的衍射峰进行放大处理 (如图 1(c) 所示) 可以看出, 随着煅烧温度的升高, 样品衍射峰强度逐渐增加, 峰形更尖锐, 表明平均晶粒明显变大. 可见高温煅烧将引起 ZnO 粒径的烧结长大.

表 1 不同样品的平均晶粒尺寸和比表面积

Table 1 Average grain size and specific surface area of the samples

Sample	Calcination temperature (°C)	Average grain size (nm)	Specific surface area (m^2/g)
ZnO	500	22.64	12.06
1% WO_3/ZnO	500	21.91	17.83
2% WO_3/ZnO	500	19.28	21.05
4% WO_3/ZnO	500	17.22	23.08
8% WO_3/ZnO	500	16.92	25.33
2% WO_3/ZnO	400	17.66	24.03
2% WO_3/ZnO	600	26.82	17.06
2% WO_3/ZnO	700	31.10	12.03
2% WO_3/ZnO	800	34.43	9.69

2.1.2 样品的比表面积

各样品的比表面积列于表 1. 可以看出, 随着 WO_3 含量的增加, WO_3/ZnO 样品的比表面积逐渐增加. 这主要是由于 WO_3 的存在使得样品粒径逐渐减小. 比表面积的增加有利于反应底物的吸附, 将提高 ZnO 的光催化活性[19]. 由 XRD 分析可知, 煅烧温度升高使得催化剂颗粒发生烧结长大, 从而导致其比表面积减小.

2.1.3 SEM 结果

图 2 为分别是 500 °C 煅烧的 ZnO, 2% WO_3/ZnO, 8% WO_3/ZnO 及 800 °C 煅烧的 2% WO_3/ZnO 的 SEM 照片. 可以看出, 500 °C 煅烧的 ZnO 颗粒之间容易团聚, 但复合 2% WO_3 后, 样品的颗粒变得更均匀, 这些小颗粒形状为球形, 大小约为 2 μm. 均匀的催化剂颗粒有利于催化剂的悬浮分散, 乃至染料分子的吸附

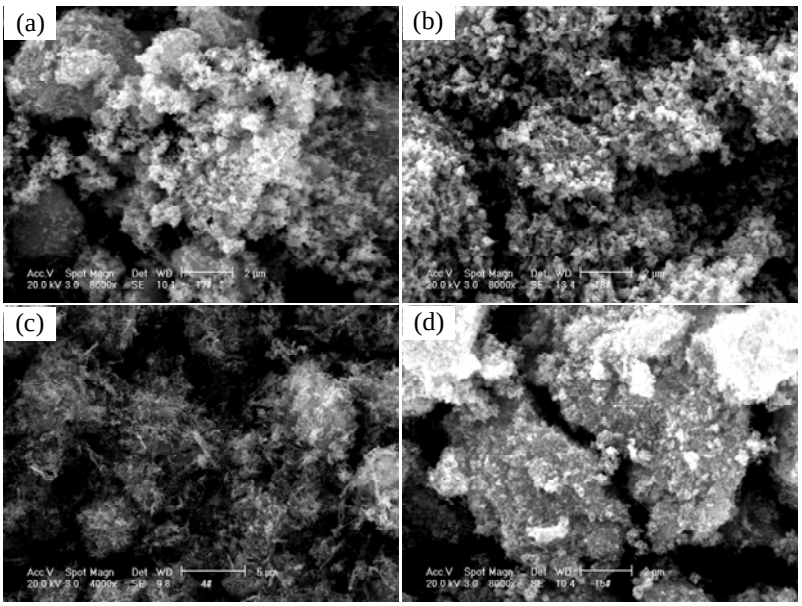

图 2 不同 WO_3/ZnO 样品的 SEM 照片

Fig. 2. SEM images of the WO_3/ZnO samples. (a) ZnO calcined at 500 °C; (b) 2% WO_3/ZnO calcined at 500 °C; (c) 8% WO_3/ZnO calcined at 500 °C; (d) 2% WO_3/ZnO calcined at 800 °C.

和光的吸收. 当 WO_3 的含量增加到 8% 时, 样品的颗粒进一步减小, 且小颗粒类似于针状, 粒子大小为 1 μm 左右. 煅烧温度升至 800 °C 时样品颗粒团聚严重. 这主要是由于煅烧温度过高, 颗粒之间发生了烧结, 粒径长大.

2.1.4 FT-IR 结果

图 3 为不同 WO_3/ZnO 样品的 FT-IR 谱. 由图可见, 所有样品均在 3440 cm^{-1} 附近出现一个宽的吸收峰, 对应于 ZnO 表面羟基的特征伸缩振动峰. 在光催化氧化反应中, 催化剂表面羟基的数量和光催化反应活性直接相关[20], 因为它不仅可以轻松地通过捕获空穴来生成羟基自由基 (·OH), 而且还可提高 O_2 对电子的捕获能力以生成更多的·OH. 另外在 1640 cm^{-1} 附近的吸收峰为游离水的 H–O–H 弯曲振动峰; 432 cm^{-1} 附近吸收峰为 Zn–O 键的特征伸缩振动峰. 由文献[21]可知, WO_3 的 FT-IR 谱在 929.2, 879.6 和 773.6 cm^{-1} 处有吸收峰. 但是在本文样品中并未出现这些吸收峰, 表明 WO_3 可能和 ZnO 产生了较强的相互作用, 导致 WO_3 的特征吸收峰消失. 由于 WO_3 或 ZnO 在 1380 与 1120 cm^{-1} 附近均无吸收峰, 而 WO_3/ZnO 样品在这两处出现的吸收峰可能是 WO_3 与 ZnO 的相互作用形成了 W–O–Zn 键而产生的峰. 还可以看出, WO_3 的存在使得表面羟基峰变宽变强, 表明复合催化剂具有更丰富的表面羟基, 这可能是由于 WO_3 的存在改善了催化剂比表面积等表面性能. 在染料分子的光催化降解反应中, ·OH 是其被氧化的主要活性物种[22]. 因此, 复合 WO_3 后, 光催化性

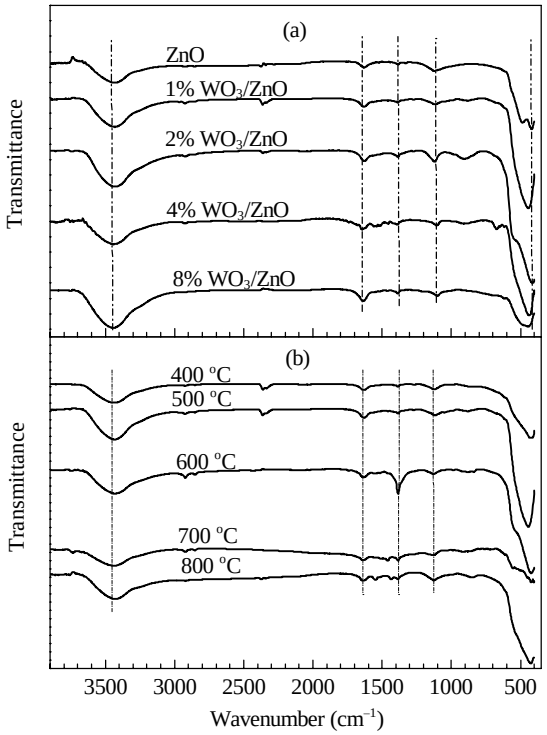

图 3 不同 WO_3/ZnO 样品的 FT-IR 谱

Fig. 3. FT-IR spectra of the samples. (a) ZnO and WO_3/ZnO with different WO_3 contents calcined at 500 °C; (b) 2% WO_3/ZnO calcined at different temperatures.

能将可能提高. 还可以看出, 随着煅烧温度的升高, 2% WO_3/ZnO样品的Zn–O–W吸收峰(1380 cm^{-1})在600 ºC时达最强, 表明在此温度煅烧, 可能加强了WO_3与ZnO的相互作用, 产生了更多的W–O–Zn键. 但当煅烧温度升到700或800 ºC时, 1380 cm^{-1}的吸收峰开始减弱, 同时在1457和1543 cm^{-1}出现了两个新吸收峰. 煅烧温度的升高使表面羟基峰(3440 cm^{-1})有所减弱, 这是由于在高温煅烧过程中样品发生了脱羟基化反应或粒子发生了烧结, 这也是导致样品比表面积减小的原因.

2.1.5 UV-Vis 结果

UV-Vis是探测半导体光学性质比较简便的方法, 它既反映样品的带隙能变化, 又可直观反映光催化材料在不同波长下对光的吸收情况. 图4为不同WO_3/ZnO样品的UV-Vis谱. 分别做它们的吸收曲线的切线与X轴相交, 得到样品的光吸收阈值λ_g, 然后根据公式 $E_g = 1240/\lambda_g$ (eV), 算出各催化剂的带隙能E_g, 结果见表2. 由图可见, ZnO纳米颗粒在λ = 200~380 nm范围内的紫外光波段有较强的吸收, 但在可见光波段几乎没有吸收能力. WO_3复合使ZnO的吸收边略向长波方向移动, 且随着复合量的增加, 红移偏移减小越明显. 这可能是由于部分W^{6+}离子形成掺杂后, 在ZnO中产生了缺陷氧空位, 因此在ZnO的导带和价带之间形成了缺陷氧能级, 从而导致吸收边发生红移[23]. 还可以看出, 煅烧温度升高, 样品的吸收边略红移.

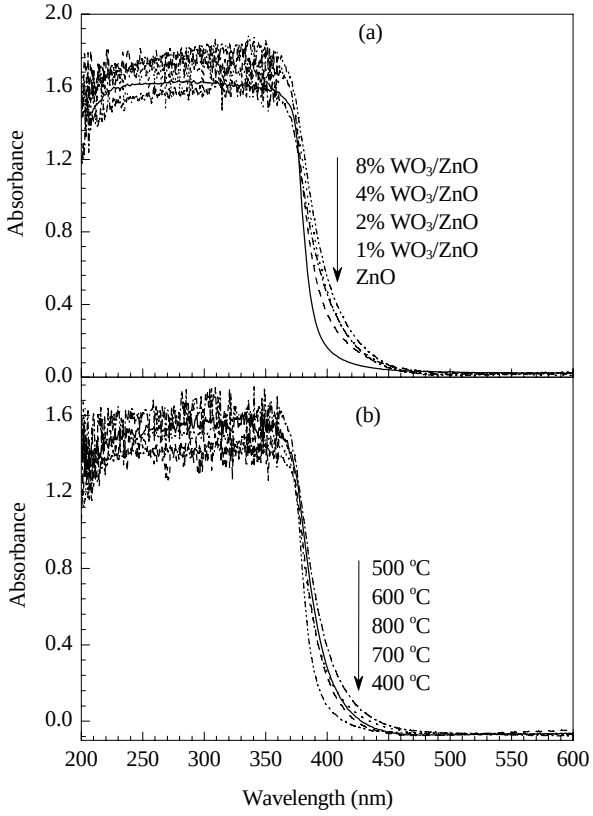

图 4 不同 WO_3/ZnO 样品的 UV-Vis 谱

Fig. 4. UV-Vis diffuse reflectance spectra of the samples. (a) ZnO and WO_3/ZnO with different WO_3 contents calcined at 500 ºC; (b) 2% WO_3/ZnO calcined at different temperatures.

表 2 不同 WO_3/ZnO 样品的带隙能

Table 2 Band gap energy of the samples

Sample	Calcination temperature (ºC)	E_g/eV
ZnO	500	3.20
1% WO_3/ZnO	500	3.03
2% WO_3/ZnO	500	2.99
4% WO_3/ZnO	500	2.93
8% WO_3/ZnO	500	2.92
2% WO_3/ZnO	400	3.13
2% WO_3/ZnO	600	3.02
2% WO_3/ZnO	700	3.02
2% WO_3/ZnO	800	3.03

2.1.6 样品的 PL 谱

为了表征复合WO_3对ZnO光催化剂光生电子与空穴对的复合的影响, 对样品进行光致发光谱分析, 结果见图5. 由文献[24]可知, ZnO纳米粒子由紫外发光峰和可见区发光带两个区域组成: (1)一个位于390 nm附近(紫外带边发射), 一般认为是ZnO的本征发光峰, 是由价带顶的空穴与导带底的电子形成的电子空穴对复合发光所引起; (2)另一个峰位于可见光区(420~620 nm), 但对该处的发光机理尚有争议, 一般认为是ZnO表面缺陷态的间接复合发光, 而该缺陷态是由于表面存在大量的不饱和键和悬键形成的. 由图可见, 复合WO_3后, WO_3/ZnO样品在可见光区域的发光峰位置没有发生变化, 但位于390 nm的紫外峰明显红移, 且随着WO_3量的增加, 紫外发光峰逐渐减弱, 表明WO_3的存在减少了ZnO表面光生电子与光生空穴的复合. 但对应的可见光发光峰的强度却增加, 这可能是由于复合WO_3后, 钨离子与ZnO的晶格氧产生相互作用, 使其不饱和键和悬键增多所致. 煅烧温度对2% WO_3/ZnO的光生电子空穴对的重组同样产生比较大的影响. 还可以看出, 随着煅烧温度的升高, 样品上红移后的紫外发光峰减弱, 其中600 ºC煅烧样品的减弱最为明显. 这可能

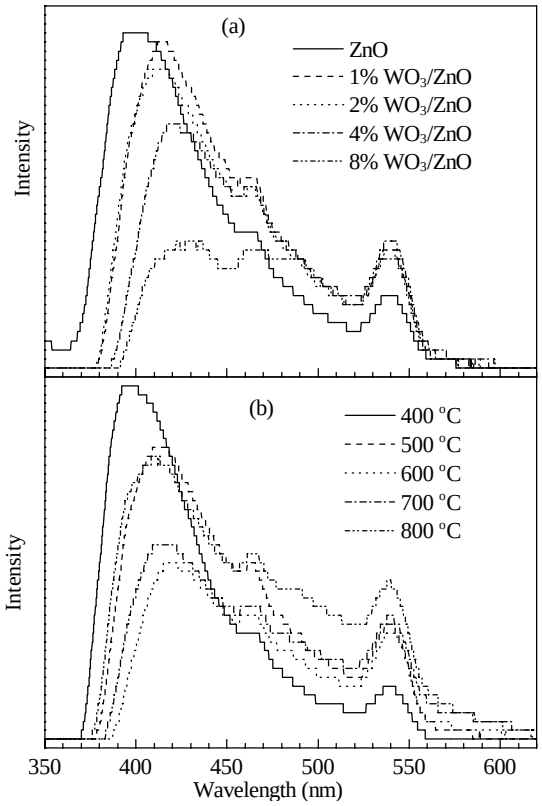

图 5 不同 WO_3/ZnO 样品的 PL 谱

Fig. 5. PL spectra of the WO_3/ZnO samples. (a) Zinc oxide and WO_3/ZnO with different WO_3 contents calcined at 500 °C; (b) 2%WO_3/ZnO calcined at different temperatures.

是由于在该温度煅烧, 提高了样品的结晶性能, 以及光生电子与光生空穴的分离效率. 但随着煅烧温度的继续提高, 该峰又有所增强, 可能是由于高温煅烧导致晶格中的氧或锌原子离开了原来的位置, 形成了更多的氧或锌空位缺陷, 导致光生电子与光生空穴复合增强. 可见发光峰的强度变化趋势是随煅烧温度升高而变强, 表明高温煅烧导致不饱和键或缺陷浓度增加了.

2.2 光催化性能和机理分析

样品的光催化活性通过在紫外光照射下降解酸性橙II模拟染料废水来测试. 图 6(a) 为不同 WO_3 含量对 WO_3/ZnO 光催化活性的影响. 由图可见, 在紫外光照射未加催化剂情况下, 酸性橙II几乎没有降解. 表明酸性橙 II 是一个稳定的染料分子, 直接光解反应可以被忽略. 随着 WO_3 含量的增加, 酸性橙 II 降解率逐渐增加, 并于 WO_3 含量为 2% 时达最大, 为 66.2%, 继续增加 WO_3 含量至 8% 时, 降解率逐渐降至 52.5%. 还可以可看出, 当样品煅烧温度从 400 °C 增到 600 °C 时, 2% WO_3/ZnO 活性增加, 主要原因是 ZnO 结晶度的提高, 减少了光生电子与空穴的复合中心, 因而光催化反应增加. 随着温度的继续升高, 光催化剂的活性又开始逐渐下降, 到 800 °C, 酸性橙 II 的降解率只有 70%. 这主要是由于 ZnO 纳米粒子烧结长大、分散性能下降, 对染料分子的吸附量大大减少, 同时比表面积减小, 不利于对反应底物分子的吸附和光的吸收.

为了定量了解不同催化剂降解酸性橙 II 实验的反应动力学, 利用 $\ln(c_0/c) = \kappa t$ 所描述的准一级动力学方程求解近似光催化降解速率常数[25,26]. 式中 c_0 和 c 是时间分别为 0 和 t 时染料溶液的浓度. 回归所得各催化剂的反应速率常数见表 3. 可以看出,

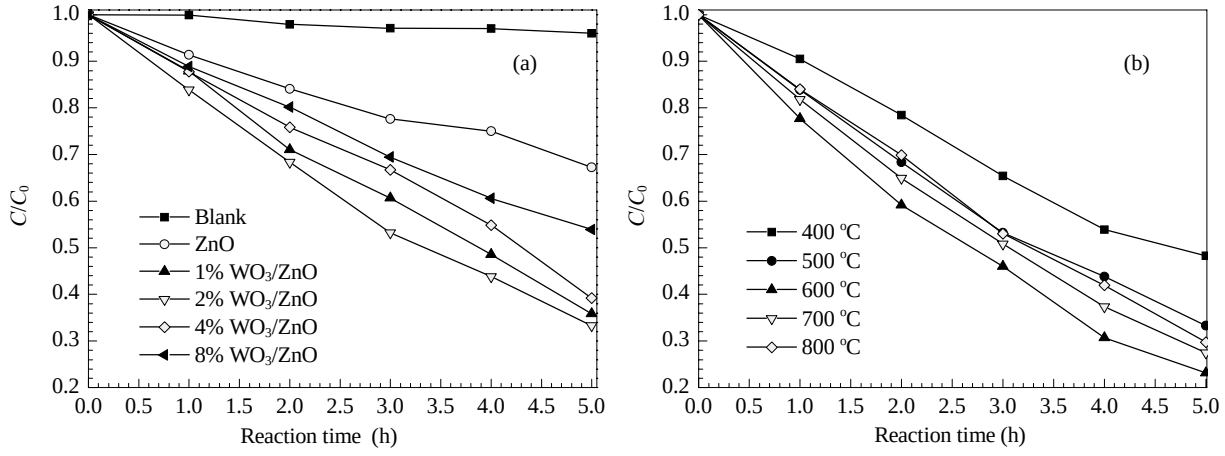

图 6 不同 WO_3/ZnO 样品降解酸性橙II的活性比较

Fig. 6. The comparison of the photocatalytic activity of ZnO and WO_3/ZnO. (a) ZnO and WO_3/ZnO calcined at 500 °C; (b) 2% WO_3/ZnO calcined at different temperatures.

表 3 不同 WO_3/ZnO 样品光催化降解酸橙 II 一级速率常数

Table 3 The first-order reaction rate constant of the catalysts in degradation of acid orange II

Sample	Calcination temperature (°C)	κ/h^{-1}	R^2
ZnO	500	0.073	0.98
1% WO_3/ZnO	500	0.218	0.99
2% WO_3/ZnO	500	0.229	0.96
4% WO_3/ZnO	500	0.194	0.99
8% WO_3/ZnO	500	0.128	0.99
2% WO_3/ZnO	400	0.163	0.99
2% WO_3/ZnO	600	0.308	0.99
2% WO_3/ZnO	700	0.274	0.99
2% WO_3/ZnO	800	0.259	0.99

$\ln(c_0/c)$ 与 t 呈良好线性关系, 相关系数 $R^2 > 0.96$, 因此该反应可表示为表观一级动力学过程. 可见, 2% WO_3/ZnO 样品于 600 °C 煅烧时, 反应速率最大为 0.308 h^{-1}.

图 7 为 WO_3/ZnO 复合光催化剂的光催化机理示意图. 如图所示, 由于 WO_3 和 ZnO 价带和导带能级位置的差异, 当它们结合在一起时, ZnO 导带中被激发的电子很容易被 WO_3 接受而迁移到其导带上, 因为 W^{6+}容易被还原成 W^{5+} [26], 成为俘获电子的中心. 同时 ZnO 价带产生的空穴可以迁移到 WO_3 的价带上去, 从而加速了光生电子和空穴的分离速率, 降低了光生电子和空穴的复合发光, 因此其光催化活性增加. 但是当复合 WO_3 超过一定限度的负载量时, 浓度过高的 WO_3 会破坏 WO_3 在 ZnO 上的分散, 且捕获载流子的捕获位间距离变小, WO_3 反而可能成为电子和空穴的复合中心, 使得光生电子-空穴分离效率降低, 故样品活性有所降低[27].

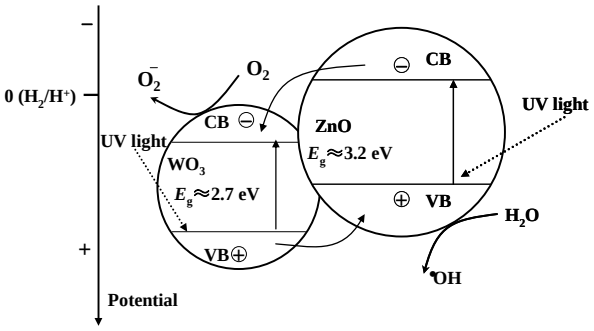

图 7 WO_3/ZnO 复合光催化剂的光催化机理

Fig. 7. Photocatalytic mechanism of the WO_3/ZnO composite photocatalyst.

3 结论

研究了不同 WO_3 含量对 WO_3/ZnO 催化剂结构、表面性质和光催化降解酸性橙 II 的性能影响. 发现 WO_3 的复合能有效地抑制 ZnO 纳米粒子的长大, 增加其比表面积, 提高表面羟基的数量, 并可有效抑制 ZnO 光生电子与空穴的复合. 当 WO_3 的含量为 2% 并在 600 °C 煅烧时, 所制催化剂的光催化活性最高, 比纯 ZnO 的光催化活性提高了约一倍.

参 考 文 献

1 Yu C L, Yu J M, Zhou W Q, Yang K. *Catal Lett*, 2010, **140**: 172
2 Yu C L, Yu J M. *Catal Lett*, 2009, **129**: 462
3 余长林, 杨凯, 余济美, 彭鹏, 操芳芳, 李鑫. 物理化学学报 (Yu Ch L, Yang K, Yu J M, Peng P, Cao F F, Li X. *Acta Phys-Chim Sin*), 2011, **27**: 505
4 Zhang J, Xu Q, Feng Z C, Li M J, Li C. *Angew Chem, Int Ed*, 2008, **47**: 1766
5 Chu DW, Masuda Y, Ohji T, Kato K. *Langmuir*, 2010, **26**: 2811
6 许平昌, 柳阳, 魏建红, 熊锐, 潘春旭, 石兢. 物理化学学报 (Xu P Ch, Liu Y, Wei J H, Xiong R, Pan Ch X, Shi J. *Acta Phys-Chim Sin*), 2010, **26**: 2261
7 李和兴, 朱建. 催化学报 (Li H X, Zhu J. *Chin J Catal*), 2008, **29**: 91
8 Xu F, Zhang P, Navrotsky A, Yuan Z Y, Ren T Z, Halasa M, Su B L. *Chem Mater*, 2007, **19**: 5680
9 Li D, Haneda H. *Chemosphere*, 2003, **51**: 129
10 Wang Y X, Li X Y, Wang N, Quan X, Chen Y Y. *Sep Purif Technol*, 2008, **62**: 727
11 韩婧, 施利毅, 成荣明, 陈奕卫, 董鹏飞, 邵启伟. 无机化学学报 (Han J, Shi L Y, Cheng R M, Chen Y W, Dong P F, Shao Q W. *Chin J Inorg Mater*), 2008, **24**: 950
12 Xu J, Chang Y G, Zhang Y Y, Ma S Y, Zhang Y Y, Ma S Y, Qu Y, Xu C T. *Appl Surf Sci*, 2008, **255**: 1996
13 傅天华, 高倩倩, 刘斐, 代华均, 寇兴明. 催化学报 (Fu T H, Gao Q Q, Liu F, Dai H J, Kou X M. *Chin J Catal*), 2010, **31**: 797
14 Wang C, Zhao J C, Wang X M, Mai B X, Sheng G Y, Peng P A, Fu J M. *Appl Catal B*, 2002, **39**: 269
15 王存, 王鹏, 徐柏庆. 催化学报 (Wang C, Wang P, Xu B Q. *Chin J Catal*), 2004, **25**: 967
16 Chen L C, Tua Y J, Wang Y S, Kan R S, Huang C M. *J Photochem Photobiol A*, 2008, **199**: 170
17 李长全, 罗来涛, 熊光伟. 催化学报 (Li Ch Q, Luo L T, Xiong G W. *Chin J Catal*), 2009, **30**: 1058
18 苏碧桃, 孙佳星, 胡常林, 张小红, 费鹏, 雷自强. 物理化学学报 (Su B T, Sun J X, Hu Ch L, Zhang X H, Fei P, Lei Z Q. *Acta Phys-Chim Sin*), 2009, **25**: 1561

19 Jing L Q, Xu Z L, Sun X J, Shang J, Cai W M. *Appl Surf Sci*, 2001, **180**: 308
20 Han X G, He H Z, Kuang Q, Zhou X, Zhang X H, Xu Tao, Xie Z X, Zheng L S. *J Phys Chem C*, 2009, **113**: 584
21 Janauer G, Dobley A, Guo J D, Zavalij P, Whittingham M S. *Chem Mater*, 1996, **8**: 2096
22 Yu C L, Yu J M, Chan M. *J Solid State Chem*, 2009, **182**: 1061
23 He Y P, Wu Z Y, Fu L M, Li C R, Miao Y M, Cao L, Fan H M, Zou B S. *Chem Mater*, 2003, **15**: 4039
24 贾铁昆, 王为民, 黄飞, 傅正义, 马秀华, 郭伟. 稀有金属材料与工程 (Jia T K, Wang W M, Huang F, Fu Zh Y, Ma X H, Guo W. *Rare Metal Mat Eng*), 2009, **38**: 979
25 Yu C L, Fan C F, Yu J M, Zhou W Q, Yang K. *Mater Res Bull*, 2011, **46**: 140
26 Tennakone K, Heperuma O A, Bandara J M S, Kiridena W C B. *Semicond Sci Technol*, 1992, **7**: 423
27 Lopez-leon T, Ortega-Vinuesa J L, Bastos-Gonzalez D, Elaissari A. *J Phys Chem B*, 2006, **110**: 4629

英 译 文

English Text

Semiconductor photocatalysis has received intensive attention in environmental purification due to its simplicity, mild reaction conditions, and low energy consumption [1–4]. ZnO is a n-type semiconductor with a band gap of 3.2 eV that is widely employed as a raw material in the textile, cosmetic, ceramic, and glass industries. ZnO has the photocatalytic ability to decompose volatile organic pollutants to CO_2 and H_2O. Organic pollutants in water can be removed by its photocatalytic degradation. Therefore, its photocatalytic ability has attracted much interest [5,6]. Compared with the common photocatalyst of TiO_2, the drawbacks of ZnO are its low efficiency of photocatalysis [7] and low stability due to photocorrosion. In order to improve its photocatalytic performance, two methods have been developed. The first is to cause changes in its physical property, such as morphology and particle size [8–10]. The second method for enhancing its photocatalytic efficiency is by noble metal deposition [11,12], metal ion doping [13], semiconductor coupling [14,15], or nonmetal element doping [16]. Among these, semiconductor coupling is an effective method to accelerate the separation of the generation of the electron (e^-)-hole (h^+) pairs because the energy gap between the two semiconductors would benefit the separation of photo-generated electrons and holes. WO_3 is another n-type semiconductor with a small band gap of 2.7 eV, and its valence and conduction band positions are different from ZnO.

In this paper, the effects of the using WO_3 in ZnO in different concentrations on the surface property and the separation efficiency of electron (e^-)-hole (h^+) pairs of ZnO were investigated. It was found that the presence of a small quantity of WO_3 can effectively enhance the photocatalytic efficiency of ZnO in the degradation of acid orange II.

1 Experimental

1.1 Catalyst synthesis

Tungstenic acid was first prepared according to the following procedure. Under stirring, 3.00 g sodium tungstate ($Na_2WO_4{\cdot}2H_2O$, AR, Sinopharm Chemical reagent Co. Ltd) and 0.05 g hexadecyl trimethyl ammonium bromide (CTAB, AR, Sinopharm Chemical reagent Co. Ltd) were dissolved in 10 ml deionized water. Then 10 ml nitric acid (1.5 mol/L) solution was slowly added into the above solution and the mixed solution was further stirred for 2 h. The precipitate produced was collected by centrifugation, washed twice with deionized water and three times with ethanol, dried in an oven at 80 °C to give the tungstenic acid. Zinc hydroxyl carbonate was prepared as follows. $Zn(NO_3)_2$ (3.67 g, AR, Shanghai, Sinopharm Chemical reagent Co. Ltd) and 0.10 g CTAB were dissolved in 50 ml deionized water to obtain solution A. Na_2CO_3 (1.31 g) was dissolved in 50 ml deionized water to obtain solution B. Solution B was added dropwise to solution A with vigorous stirring. After stirring for 1 h, the precipitate was collected by the same method as above. Then, an appropriate amount of tungstenic acid was mixed with zinc hydroxyl carbonate and the mixture was ground for 0.5 h. The mixture was calcined at different temperatures for 2 h in air. The final contents of W and other elements in the composite were determined by X-ray fluorescence analysis (Panalytical-PW2424).

1.2 Catalyst characterization

The BET surface areas of the samples were obtained from N_2 adsorption-desorption isotherms determined at liquid nitrogen temperature (–196 °C) on an automatic analyzer (NOVA 4000).The samples were outgassed for 2 h under vacuum at 350 °C prior to adsorption. X-ray diffraction (XRD) patterns were obtained on a Bruker D8 Advance X-ray diffraction meter using Cu K_α radiation (λ = 0.154178 nm) at a scan rate of 0.05°/s. The accelerating voltage and the applied current were 30 kV and 15 mA, respectively. The microstructures of the samples were determined by a XL30 (Philips) scanning electron microscope (SEM) with an energy dispersive X-ray (EDX) spectrometer (EDax Genesis instrument, USA). UV-Vis diffuse reflectance spectra (DRS) were measured using a UV-Vis spectrophotometer (UV-2550, Shimadzu). Absorption spectra were referenced to $BaSO_4$. Fourier transform infrared (FT-IR) spectra were recorded with a Nicolet 470 FTIR spectrometer (USA).

Samples were pressed by a KBr disk preparation apparatus. The samples were dried at 250 °C for 4 h prior to pressing. To investigate the recombination and lifespan of photo-generated electrons/holes in the photocatalysts, the photoluminescence (PL) emission spectra of the samples were recorded. A 325 nm He-Cd laser was used as an excitation light source. The emission from the sample was measured by a spectrometer (Spex 500M, USA) equipped with a photon counter (SR400, USA).

1.3 Photocatalytic activity test

The photocatalytic activities of the samples were determined by measuring the degradation of acid orange II in an aqueous solution under UV light irradiation. A 365-nm UV lamp (15 W Cole-Parmer Instrument Co.) was used as light source. The photocatalyst (0.05 g) was suspended in 80 ml aqueous solution of C_0 = 0.020 g/L. Before the lamp was turned on, the suspension was stirred in the dark for 40 min. The suspension was vigorously stirred in the photoreactor during the process and the temperature of suspension was maintained at (22±2) °C by the circulation of water through an external cooling coil. After fixed intervals of illumination, a sample of the suspension was taken out and centrifuged. The clear upper layer solution was analyzed by a spectrophotometer. The dye concentration was measured at λ = 484 nm, which is the maximum absorption wavelength for acid orange II. The degradation rate (D) of acid orange II was calculated according to the equation $D = (A_0 - A)/A_0$ (A_0: initial absorption degree; A: final absorption degree).

2 Results and discussion

2.1 Characterization analysis

2.1.1 XRD analysis

XRD patterns were used to determine the effects of the addition of WO_3 on the crystal phase and crystallinity of ZnO. Figure 1(a) shows the XRD patterns of pure ZnO and WO_3/ZnO samples with different WO_3 concentration. The diffraction peaks of the (100), (002), (101), (102), (110), (103), (200), (112), and (201) crystal planes were well indexed with JCPDS 36-1451, which indicated that the ZnO has the hexagonal wurtzite structure and high crystallinity. With all the samples, no diffraction peak of WO_3 can be observed, which may due to the highly dispersed WO_3 or low concentration of WO_3 below the XRD detection limit [17]. The effects of calcination temperature on the crystallinity of 2% WO_3/ZnO are shown in Fig. 1(b). The position of the diffraction peaks showed no changes, which indicated no new compound was formed. With increase of calcination temperature, the intensity of the diffraction peak at (101) became stronger, suggesting the increase of crystallinity.

The Scherrer equation was used to estimate the average crystallite sizes of the samples. The results are summarized in Table 1. Table 1 shows that the addition of WO_3 decreased the crystal size of ZnO, which indicated that the presence of WO_3 restrained the growth of ZnO nano-particles. The possible reason for this could be that some W^{6+} entered into the crystal lattice of ZnO and suppressed the growth of the ZnO crystal due to the similar radius of W^{6+} (0.068 nm) and Zn^{2+} (0.083 nm) [18]. The larger diffraction peaks at 36.4° for 2% WO_3/ZnO calcined at different temperatures showed that the intensities of these peaks increased gradually with the increase in temperature from 400 to 800 °C, which also indicated that an elevated temperature calcination will cause the sintering of ZnO particles and increase the crystallite size.

2.1.2 BET surface area analysis

The BET surface areas of all the samples are also shown in Table 1. The specific surface area of the WO_3/ZnO samples increased with the increase of WO_3 content, which was mainly caused by the decrease of the crystallite size of ZnO due to the presence of WO_3. The increase of surface area will benefit the adsorption of dye and increase the photocatalytic activity of ZnO [19]. The XRD analysis showed that the increase of calcination temperature caused the sintering of ZnO particles, thus resulting in the decrease of surface area.

2.1.3 SEM analysis

The morphologies and dispersions of the samples were determined by SEM. Figure 2 shows typical SEM images. Figure 2(a) indicates that the ZnO particles calcined at 500 °C had aggregated somewhat. However, the addition of 2% WO_3 resulted in a better and uniform dispersion for this sample, as shown in Fig. 2(b). The particles in this sample have a sphere-like morphology with a size of around 2 μm. The uniform size of the catalyst particle can benefit catalyst dispersion, adsorption of dye and light absorption in this photocatalytic system. Figure 2(c) shows the SEM image of 8% WO_3/ZnO, which shows that the increase of WO_3 content further decreased the particle size of this sample. These particles showed a needle-like morphology with a size of about 1 μm. Figure 2(d) shows that serious aggregation of the particles took place when the sample was calcined at 800 °C with sintering of the particles.

2.1.4 FT-IR analysis

Figure 3 gives the infrared spectra of all the samples. All the samples have a peak at 3443 cm^{-1}, which was assigned to

the stretching vibration and bending vibration of surface –OH groups on ZnO. In the photocatalytic reaction, the reaction activity is closely related to the amount of –OH groups on the catalyst because the –OH groups can capture the photo-generated hole (h^+) and transform to reactive $^{\bullet}OH$ radicals. The peak at 1630 cm^{-1} was assigned to the bending vibration of adsorbed water on the surface of the catalyst. The peak at 432 cm^{-1} was attributed to the stretching vibration of the Zn–O bond. From the literature [21], it is known that the characteristic peaks for WO_3 are at 929.2, 879.6, and 773.6 cm^{-1}. However, with all the samples, no peak for WO_3 was observed. A strong interaction between WO_3 and ZnO may be the cause of the non-appearance of the characteristic peaks of WO_3. Another two peaks at 1380 cm^{-1} and 1120 cm^{-1} could be ascribed to the formation of a W–O–Zn bond because these two peaks were not found with WO_3 and ZnO. Figure 3(a) shows that the addition of WO_3 caused the peak at 3443 cm^{-1} to become stronger and bigger, which suggested that more –OH groups may be present due to the increase of surface area and the improved property of the surface. In the photocatalytic degradation of the dye, the main reactive radical is $^{\bullet}OH$ [22]. Therefore, the presence of WO_3 can effectively improve the photocatalytic activity. Figure 3(b) also shows that at the same concentration of WO_3, with the increase in calcination temperature from 400 to 600 °C the intensity of the peak at 1380 cm^{-1} increased gradually, which indicated that in this temperature range, the increase in calcination temperature can strengthen the interaction between WO_3 and ZnO and produce more W–O–Zn bonds. However, when the calcination temperature was increased to 700 and 800 °C, the intensity of this peak began decreasing. At the same time, two new peaks at 1457 and 1543 cm^{-1} appeared. The high calcination temperatures decreased the intensity of the peak at 3443 cm^{-1} because the elevated temperature treatment caused the loss of –OH groups and surface area.

2.1.5 UV-Vis diffuse reflectance spectra

UV-Vis diffuse reflectance spectroscopy is an effective technique to determine the light absorption ability of a semiconductor at different wavelengths. Figure 4 shows the UV-Vis diffuse reflectance absorption spectra of all the samples. The band gap energy (E_g) for the catalyst was determined with $E_g = 1240/\lambda_g$ (eV), where λ_g is the absorption edge, which was obtained from the intercept between the tangent of the absorption curve and the abscissa. The calculated band gap energies for the different samples are shown in Table 2. Figure 4(a) shows that pure ZnO has strong light absorption from 200 to 380 nm and no absorption in the visible light range. The presence of WO_3 caused the absorption to shift towards long wavelengths, which may be due to the formation of the energy level of vacancy oxygen because when W^{6+} was doped into the crystal lattice of ZnO, an vacancy oxygen may form [23]. Figure 4(b) indicates that the calcination temperatures had slight influences on the light absorption of 2% WO_3/ZnO. The increase in temperature caused the absorption edge to slightly shift to long wavelengths.

2.1.6 PL emission spectra

PL emission spectra were used to investigate the effects of the coupling of WO_3 on the recombination of photo-generated electrons and holes in ZnO. According to the literature [24], two emission peaks of ZnO can be observed. One is around 390 nm near the ultraviolet range, which is due to the recombination of photo-generated electrons and holes. Another emission peak is around 420–620 nm; there is some controversy about the mechanism of this emission. One explanation is that this emission is an indirect emission which is related to a surface vacancy on ZnO. Figure 5(a) shows that the addition of WO_3 did not change the position of the emission peak in the visible light range. However, a red shift occurred for the emission peak at 390 nm due to the presence of WO_3. Moreover, an increase in WO_3 content caused a decrease in the intensity of this emission peak, which suggested that the recombination of photo-generated electrons and holes was effectively suppressed by the WO_3. As for the emission peak in the visible light range, a slight increase in its intensity appeared with the existence of WO_3. A possible reason is that an interaction between W^{6+} and crystal lattice oxygen resulted in an unsaturated bond and surface vacancy on ZnO. The calcination temperature had a big influence on the recombination of photo-generated electrons and holes. An increase in calcination temperature from 400 to 600 °C caused the decrease on the intensity of the emission peak at 390 nm, which was because the increased crystallinity enhanced the separation of photo-generated electrons and holes. Therefore, the sample calcined at 600 °C showed the smallest intensity. However, the further increase in temperature from 600 to 800 °C increased the intensity of this emission peak. The very high temperature may result in the displacement of O^{2-} and Zn^{2+} and produce more O^{2-} or Zn^{2+} vacancy in the ZnO crystal lattice. The vacancy would increase the recombination of photo-generated electrons and holes. As for the emission peak in the visible light range, the increase in temperature slightly increased the intensity of this emission peak.

2.2 Photocatalytic activity test and enhancement mechanism

The photocatalytic activities of the samples were evalu-

ated by measuring the decomposition of acid orange II in an aqueous solution under UV light (λ = 365 nm) irradiation. Figure 6(a) shows the effects of WO_3 content on the photocatalytic activity. It was found that acid orange II was only slightly degraded under light irradiation without a catalyst, indicating that acid orange II is a stable molecule and its photolysis can be ignored. The increase of WO_3 from 0 to 2% effectively increased the degradation efficiency. However, the further increase of WO_3 gave an adverse effect. The degradation rates of acid orange II after 5 h of irradiation over ZnO, 1% WO_3/ZnO, 2% WO_3/ZnO, 4% WO_3/ZnO and 8% WO_3/ZnO were 40.86, 64.18, 66.18, 60.79, and 52.52%, respectively. The optimal concentration of WO_3 was found 2%.

Figure 6(b) gives the effects of calcination temperature on the photocatalytic activity of 2% WO_3/ZnO. From 400 to 600 ^oC, the increase in temperature gave a big increase in activity, which was due to that the recombination of photo-generated electrons and holes was suppressed by the increase in crystallinity. The further increase in temperature produced a negative effect on activity. The sample calcined at 800 ^oC only gave 70% degradation rate. The elevated temperature calcination caused the sintering of the catalyst. The loss of surface area, increase in crystalline size, and decrease in dispersion all gave an adverse effect on the harvest of light and the adsorption of dye.

To quantitatively understand the reaction kinetics of the acid orange II degradation in our experiments, we used a pseudo-first order model expressed by the equation $\ln(C_0/C) = \kappa t$, which can be generally used for photocatalytic degradation if the initial concentration of the pollutant is low [25,26]. C_0 and C are the concentrations of dye in the solution at time 0 and t, respectively, and κ is the pseudo-first order rate constant. The rate constants obtained from the regression of $\ln(C/C_0)$ vs t are shown in Table 3. A good correlation with pseudo-first order reaction kinetics (R^2 > 0.96) was found. The highest reaction rate constant was 0.308 h^{-1} for the sample calcined at 600 ^oC with 2% WO_3.

A simple mechanism shown in Fig. 7 is suggested. WO_3/ZnO can be considered a coupling of two semiconductors. Due to the different positions of the valence and conduction bands of WO_3 and ZnO, excited electrons in the conduction band of ZnO can easily transfer to the conduction band of WO_3 because W^{6+} can capture electrons and be reduced to W^{5+} [26]. At the same time, the holes in the valence band of WO_3 can transfer to the valence band of ZnO. Therefore, the recombination of the photo-generated carriers is suppressed, leading to an increase in the photo-oxidation efficiency. However, if the WO_3 content is too high, the dispersion of WO_3 would become poor and the redundant WO_3 can become recombination centers, resulting in a decrease in photocatalytic activity [27].

3 Conclusions

The effects of the addition of different WO_3 contents on the properties of the structure and surface of ZnO and its photocatalytic activity in the degradation of acid orange II were investigated. The presence of WO_3 can effectively suppress the growth of ZnO particles and increase its surface area and $^{\cdot}OH$ groups. The recombination of photo-generated electrons and holes was also suppressed. The sample with 2% WO_3 calcined at 600 ^oC was twice as active as pure ZnO.

Full-text paper available online at ScienceDirect
http://www.sciencedirect.com/science/journal/18722067